

Human Arm Pose Estimation with a Shoulder-worn Force-Myography Device for Human-Robot Interaction

Rotem Atari, Eran Bamani and Avishai Sintov

Abstract—Accurate human pose estimation is essential for effective Human-Robot Interaction (HRI). By observing a user’s arm movements, robots can respond appropriately, whether it’s providing assistance or avoiding collisions. While visual perception offers potential for human pose estimation, it can be hindered by factors like poor lighting or occlusions. Additionally, wearable inertial sensors, though useful, require frequent calibration as they do not provide absolute position information. Force-myography (FMG) is an alternative approach where muscle perturbations are externally measured. It has been used to observe finger movements, but its application to full arm state estimation is unexplored. In this letter, we investigate the use of a wearable FMG device that can observe the state of the human arm for real-time applications of HRI. We propose a Transformer-based model to map FMG measurements from the shoulder of the user to the physical pose of the arm. The model is also shown to be transferable to other users with limited decline in accuracy. Through real-world experiments with a robotic arm, we demonstrate collision avoidance without relying on visual perception.

I. INTRODUCTION

Human-Robot Interaction (HRI) within a shared workspace involves either coexistence or collaborative interaction. In coexistence scenarios, humans and robots work independently on distinct tasks while avoiding each other [1]. In collaborative interaction, they interact dynamically to accomplish a shared goal [2]. Both scenarios require the robot to accurately understand and anticipate the human’s intentions and arm movements in real-time. Applications can include medical procedures [3], rehabilitation [4], factory assistance [5] and domestic robotics [6]. In these scenarios, the robot’s ability to observe human motion and respond is crucial for effective interaction.

We consider the problem of estimating the current pose of the entire human arm. Estimation models are usually based on either visual perception or wearable devices. The most notable approach for the former is the use of human pose estimation models (i.e., *Skeleton* models [7], [8]). Such a model locates key points (e.g., head, shoulders, elbows, wrists, hips and knees) on a human body within an image or video, that can be used to reconstruct a person’s pose in 2D or 3D space. Hence, a camera can observe the user, estimate arm poses in real-time, and proactively initiate actions to avoid collisions or plan task completion [9]. However, the sole reliance on continuous visual feedback can hinder task performance in scenarios with visual uncertainty, such as

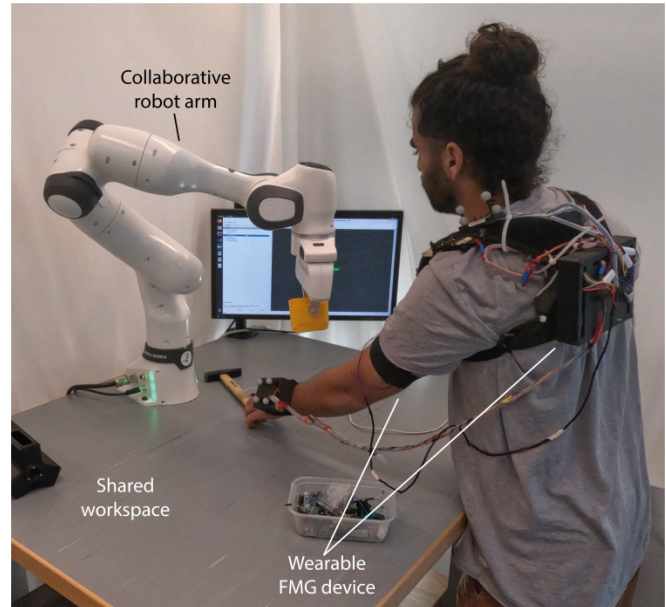


Fig. 1. A user is working in a share workspace with a robotic arm. A wearable Force-Myography (FMG) device is used to estimate the pose of the human arm in real time. In this example, when the user reaches to pick up a tool, the robot halts its motion to avoid interference and potential collisions.

poor lighting, occlusions, long distance and multiple users in the scene. Additionally, visual sensing demands substantial data and computational resources [10], potentially limiting its practicality in certain applications.

To cope with the vision limitations, wearable technology has been proposed with sensing modalities such as Electro-Myography (EMG) [11] and Ultrasound [12]. In general, estimating arm poses solely through wearable sensing can enhance the robustness of HRI systems, particularly in challenging environments with limited or occluded visual information. Later, potential fusing of wearable sensor data with visual inputs can achieve more accurate and reliable pose estimation. The prominent approach is the use of body-worn Inertial Measurement Units (IMU) [13]. Typically, one or two IMU sensors are placed on the user’s arm and used to estimate arm pose [14]–[16]. IMUs typically combine accelerometers, gyroscopes and magnetometers, and can be used to estimate kinematic data such as velocity, position and orientation. These estimations are often jeopardized by noise and drift. Kalman filtering and machine learning techniques are commonly employed to address these challenges and improve the accuracy of the estimated motion [17]. However,

R. Atari, E. Bamani and A. Sintov are with the School of Mechanical Engineering, Tel-Aviv University, Israel. Corresponding Author: sintov1@taux.tau.ac.il.

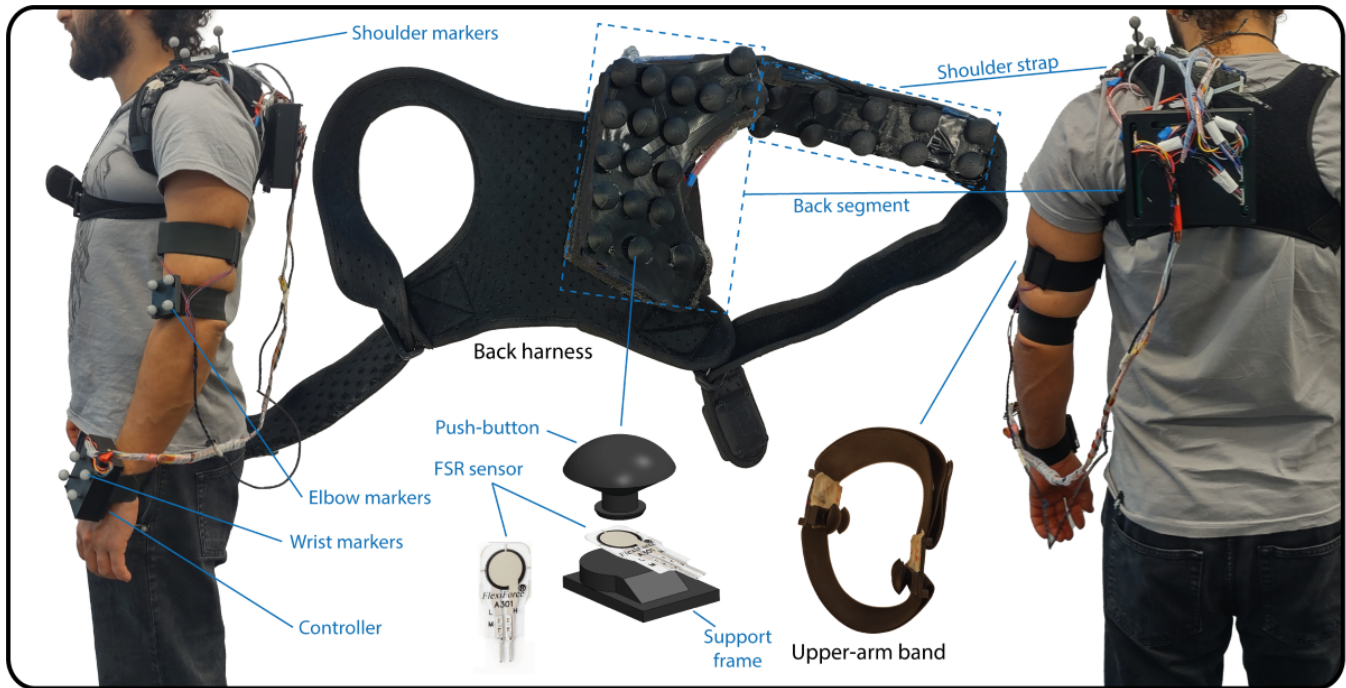


Fig. 2. The wearable FMG device includes a back harness and an upper arm band, with a total of 32 FSR sensors. Reflective markers are fixed on the shoulder, elbow and wrist for data collection.

IMU-based estimations require frequent calibration as they provide relative, rather than absolute, measurements [18]. With similar calibration requirements, IMUs were also used to predict the future target of the users arm for seamless HRI [19], [20].

Force-Myography (FMG) is a non-invasive technique for measuring muscle activity [21]. FMG involves placing simple force sensors on the skin to monitor muscular contractions and relaxations. Compared to EMG, FMG is known for its ease of acquisition, high accuracy and robustness to positioning variations [22], [23]. FMG offers a better signal-to-noise ratio and anti-interference ability, providing more stable signals with resistance to interference such as sweating and electromagnetic disturbances [24]. In addition, FMG technology utilizes simple force-sensitive resistors, resulting in a low-cost device. These advantages have led to its successful application in rehabilitation studies [25], teleoperation [26], prosthetics [27], [28], and classification of hand gestures [29] and held objects [30], [31]. In all of these applications, FMG sensing was conducted on the forearm of the user and, thus, usually provides only information regarding the state of the hand and fingers. To the best of the authors' knowledge, FMG sensing has not been previously applied to model the complete state of the human arm, and specifically by measuring perturbations of shoulder muscles.

In this letter, we explore the feasibility of utilizing FMG for comprehensive modeling of the human arm, with the goal of natural HRI. In a novel approach, FMG sensors are strategically placed on the upper back, shoulder and arm,

enabling the acquisition of data that can be used to infer arm pose. This is the first application of FMG on shoulder muscles and for modeling the state of the entire human arm. To estimate the instantaneous pose, we propose a novel approach utilizing the Transformer architecture [32], leveraging its ability to process temporal sequential data effectively. We then demonstrate its use in an HRI scenario where a robot must perform its own task without interfering or colliding with the human user. Unlike the relative positioning of IMUs, FMG offers absolute positioning with respect to the human torso without the need for constant calibration. Hence, it can be integrated in the future to the clothing of users, enabling seamless sensing and data collection in various applications.

This work pioneers the use of FMG for full-arm pose estimation, enabling robust human-robot interaction. Key contributions include:

- *Novel FMG Application:* We introduce a novel approach to FMG, positioning sensors on the shoulder to capture arm pose information.
- *Transformer-based Model:* We propose a Transformer-based model to effectively map FMG signals to accurate arm pose estimates.
- *Cross-User Generalization:* We demonstrate the model's ability to generalize to new users, even with varying body dimensions.
- *Real-world Validation:* The model's effectiveness is validated in real-world HRI scenarios with a collaborative robot arm.

While our focus is on robotic arm collaboration, the proposed

approach can also be adapted for applications involving prosthetic hands, drones, teleoperation, and virtual reality.

II. METHOD

A. Problem Statement

We consider a shared workspace denoted by $\mathcal{W} \in \mathbb{R}^3$. It is assumed that the body pose of the human user in front of \mathcal{W} is known and relatively static. The general problem involves enabling a robot to estimate the pose of a human arm within the shared workspace, with the aim of facilitating collaborative tasks or avoiding collisions. The state of the user's arm is represented by the tuple $\mathbf{v} = \{\mathbf{p}_{el}, \mathbf{p}_{wr}\} \in \mathcal{P}$ where $\mathcal{P} \subset \mathbb{R}^3 \times \mathbb{R}^3$ and is composed of the spatial positions $\mathbf{p}_{el} \in \mathbb{R}^3$ and $\mathbf{p}_{wr} \in \mathbb{R}^3$ of the elbow and wrist, respectively. The positions are measured with respect to the position of the shoulder $\mathbf{p}_{sh} \in \mathbb{R}^3$. Furthermore, an FMG device is positioned on the shoulder and upper arm of the user. Hence, let $\mathbf{x} \in \mathbb{R}^n$ represent the state of the musculoskeletal system, which is captured through the n FMG signals acquired from the FMG device. We search for a mapping $\Gamma : \mathcal{C} \rightarrow \mathcal{P}$ where \mathcal{C} is some product of the FMG space in \mathbb{R}^n . Map Γ should approximate the state of the human arm with respect to the body based on the FMG data.

B. FMG System

The proposed FMG device is based on a back harness and an upper arm band with a total of $n = 32$ Force-Sensitive Resistors (FSR) model FlexiForce A301. FSR sensors are polymer films that exhibit changes in electrical resistance when subjected to varying pressure. Each FSR sensor is equipped with a push-button mechanism. The button has a spherical design to allow better attachment onto the muscle and a larger surface area, maximizing the amount of information extracted from each muscle group. This adaptability accommodates the variations in the user's skin even when the surface is uneven. All FSR sensors are connected to an Arduino Uno micro-controller through a voltage divider of $150k\Omega$. This configuration enables real-time reading of the sensors at a maximum stable frequency of 100 Hz, yielding similar sampling frequency.

The back harness is comprised of 28 FSR and is tightened to the back using shoulder straps. The FSR sensors on the harness's dorsal cover the upper back of the user at the shoulder of the measured arm as seen in Figure 2. The back segment of the dorsal covers, with 18 FSR sensors, the Infraspinatus muscle and the back side of the Trapezius muscle [33]. In addition, 10 FSR sensors are aligned on the shoulder strap and sense the top of the Trapezius muscle. The separated band with four sensors is wrapped around the upper arm and sense perturbations of the triceps with four FSRs. All FSR sensors are distributed in relatively equal spacing and in tabular formations within each section.

To collect labeled data, a motion capture (MoCap) system was used to measure \mathbf{v} . Therefore, reflective markers were positioned on the shoulder, elbow and wrist of the measured arm. They were measured with respect to the coordinate frame of \mathcal{W} determined in the calibration of the MoCap.

Then, the positions of the elbow and wrist with respect to the shoulder can be computed by simple subtraction, making them independent of any environment. Consequently, an FMG measurement \mathbf{x}_i can be labeled by an arm state \mathbf{v}_i .

C. Data Collection

Train and test datasets were collected by synchronously recording FMG signals with the three key points on the human arm. This research investigates the feasibility of training an accurate Γ model using data from only a single participant and potentially transferring it to novel users. To achieve this, data was collected from a single participant across K separate sessions and M samples per session. In each session, the device was taken off and re-worn to include variations in sensor placement and tightening forces.

During each session, the participant was instructed to perform a diverse set of arm movements within the front workspace. These movements included scanning through the space with varied arm postures and velocities, flexing and extending the arm at different elbow positions and velocities, reaching to different target locations, and holding a range of static postures. Hence, the participant comprehensively explores the full arm range of motion, ensuring that both high and low velocity movements were captured across a wide array of configurations. This approach allows the dataset to accurately represent fine muscle movements as well as gross motor actions. The resulting dataset is a set of $N = KM$ labeled FMG measurements $\mathcal{Q} = \{(\mathbf{x}_i, \mathbf{v}_i)\}_{i=1}^N$. A similar test dataset was collected in independent sessions for evaluating trained models.

D. Pose Estimation Model

We now aim to train a data-based model Γ to acquire pose estimation based on FMG data. We hypothesize that a temporal analysis of FMG signals can enhance arm pose estimation. This assumption is grounded in the belief that FMG signals vary with arm velocities, and temporal sequences can effectively embed these variations. We define the space of temporal FMG sequences by $\mathcal{C}_H \subset \mathbb{R}^n \times \dots \times \mathbb{R}^n$ where H is the length of the sequence. Therefore, sequential batches of length H are extracted from dataset \mathcal{Q} and labeled with the corresponding pose based on the last signal in the sequence. Let $\mathbf{x}(t)$ and $\mathbf{v}(t)$ be the FMG and arm states, respectively, at time t . Hence, an FMG sequence

$$\mathbf{c}(t) = \{\mathbf{x}(t-H), \dots, \mathbf{x}(t)\} \in \mathcal{C}_H \quad (1)$$

corresponding to time t is labeled by $\mathbf{v}(t)$. The sequences are sampled using a sliding window over the episodes in \mathcal{Q} with step size $H/2$ to ensure diversity. This step size assists in reducing data redundancy while maintaining the temporal structure. Similar sampling is done to the test set but with a window step size of 1. The pre-processing step yields a modified dataset $\mathcal{Q}' = \{(\mathbf{c}_i, \mathbf{v}_i)\}_{i=1}^W$ where the number of sequences W depends on H and N . Consequently, we search for a map $\Gamma_\theta : \mathcal{C}_H \rightarrow \mathcal{P}$ where H is an hyper-parameter to be optimized and θ is the trainable weight vector of the model.

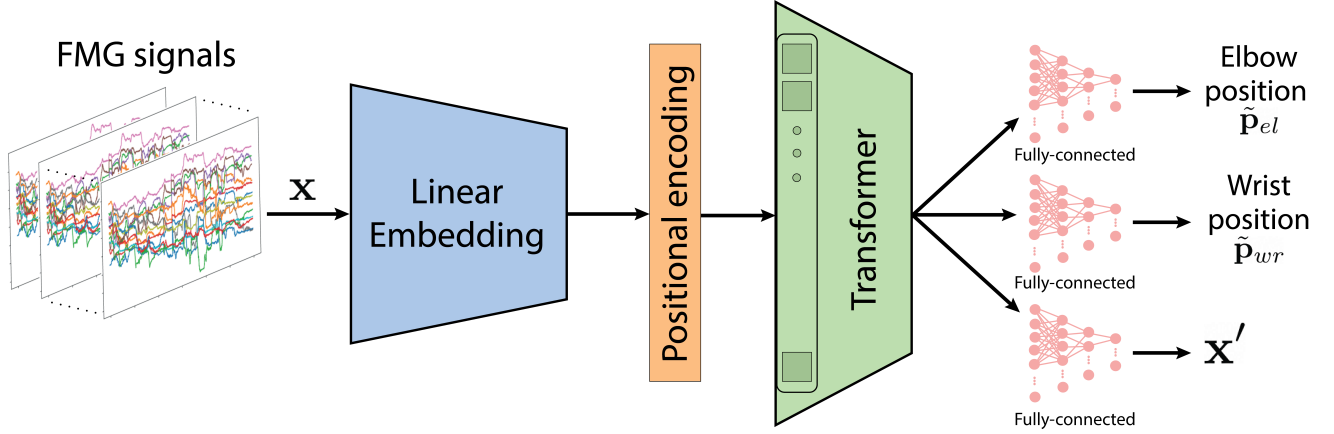


Fig. 3. Illustration of the Transformer-based model for mapping temporal FMG signals to the positions of the elbow and wrist.

Mapping Γ_θ can be formulated as a multivariate time series representation learning problem, where the goal is to map a temporal FMG signal $\mathbf{c}(t)$ to the arm pose $\mathbf{v}(t)$. While sequential modeling can be done using models such as Recurrent Neural Networks (RNN) [34] or Convolutional Neural Networks (CNN), Transformers have emerged in the last few years as a powerful and data efficient tool for modeling sequential data such as language and time series [32]. The success of the Transformer can be attributed to its ability to model long-range dependencies using a multi-head attention mechanism, which allows it to attend to different time steps simultaneously. Unlike RNN-based models that process data sequentially, Transformers process all input data at once, making them well-suited for tasks where long-term dependencies are important. This capability is particularly beneficial for FMG data, which requires learning complex dependencies between muscle activity and arm movements. Therefore, we base our Γ_θ model on the Transformer Encoder architecture and later compare it to other existing data-based models.

Our model, illustrated in Figure 3 consists of an embedding layer that maps the input data into a space of dimension d_{model} . A positional encoding layer is applied to inject information about the sequence order into the model. The model includes a transformer encoder with multiple layers, each comprising a multi-head attention mechanism, a feed-forward network with d_{ff} hidden layers and ReLU activation after each layer. Dropout is applied after each attention and feed-forward sub-layer. The output of the Transformer is passed through a series of fully connected layers, each reducing the dimensionality of the feature space, yielding the final position estimation outputs $\tilde{\mathbf{p}}_{el}$ and $\tilde{\mathbf{p}}_{wr}$. In addition, the output of the Transformer is passed through another fully-connected network outputting \mathbf{x}' , the reconstruction of the FMG input \mathbf{x} . The Transformer-based model is trained in two phases [32]. In the first phase, the model is trained in an unsupervised manner where the positional outputs are ignored and the reconstruction loss $\mathcal{L} = \|\mathbf{x} - \mathbf{x}'\|$ is minimized. In the second phase, supervised learning is

employed to minimize the loss given by

$$\mathcal{L} = \frac{1}{J} \sum_i^J \{(\tilde{\mathbf{p}}_{el,i} - \mathbf{p}_{el,i})^2 + (\tilde{\mathbf{p}}_{wr,i} - \mathbf{p}_{wr,i})^2\} \quad (2)$$

where $\tilde{\mathbf{p}}$ and \mathbf{p} are the predicted and ground-truth positions, respectively, and J is the number of samples in the batch.

III. EXPERIMENTS

In this section, we evaluate the FMG-based arm pose estimation model and the ability of the model to be used in a shared workspace within an HRI scenario. The data collection and experiments were conducted with the approval of the ethics committee at Tel-Aviv University under application No. 0007829. All models were trained with an NVIDIA GeForce RTX 3060 Ti GPU. Hyperparameter tuning was performed using Ray-Tune [35], optimizing the model parameters across multiple configurations. Videos of data collection and experiments can be seen in the supplementary material.

A. Dataset

Data was collected as described in Section II-C on a single human subject. The user contributed data across $K = 48$ sessions with $M = 20,000$ average samples per session. Between each session, the FMG device was removed and re-positioned. In addition, the participant's torso was kept in an upright, fixed position to minimize torso movement, thus isolating the analysis to arm movements. The collection yielded a total of approximately $N = 10^6$ samples in \mathcal{Q} . In addition, a separate and independent test set was collected with 40,000 samples over two sessions. Then, the dataset was processed into temporal series with horizon $H = 128$ leading to $W = 7,306$ temporal sequences in \mathcal{Q}' . The value for H was chosen based on hyper-parameter optimization. A similar test set was generated with 19,371 labeled sequences.

B. Model Evaluation

In this section, we analyse the Transformer-based model. First, we compare our proposed model to other existing

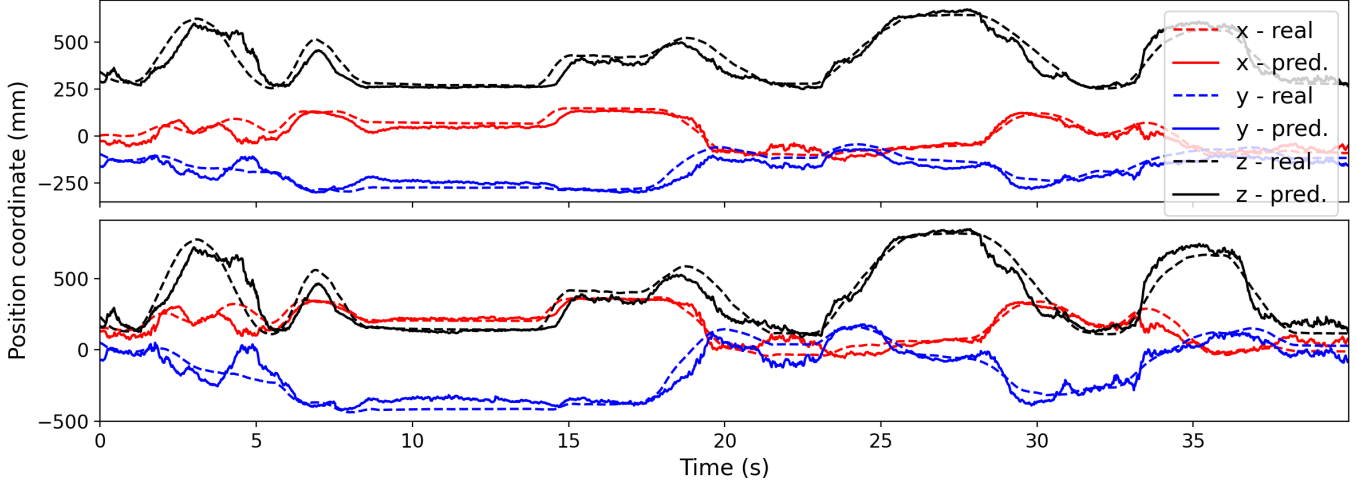


Fig. 4. Real and predicted positions of the (top) elbow and (bottom) wrist, with regard to motion time.

TABLE I
EVALUATION METRICS FOR DIFFERENT MODELS

Model	Position error (mm)		Inference time (ms)
	Elbow	Wrist	
FC-NN	73 ± 60	143 ± 33	0.37
1DCNN	71 ± 55	140 ± 55	0.27
DLinear	81 ± 80	153 ± 80	5.7
CNN-LSTM	67 ± 65	138 ± 65	0.88
Transformer	60 ± 60	120 ± 33	1.3

models including Fully-Connected Neural Network (FC-NN), 1DCNN [36], DLinear [37] and Long Short-Term Memory with CNN (CNN-LSTM) [38].

The FC-NN is the baseline where the temporal data is flattened to a $n \times H$ vector and fed into a series of fully-connected layers. 1DCNN is a type of CNN specifically designed for processing sequential data, such as text or time series. It applies filters to input sequences to extract relevant features and learn patterns. DLinear is a deep linear model designed for forecasting long-term time series and combines the strengths of linear models with the flexibility of deep architectures. It uses a linear transformation to capture temporal dependencies while maintaining computational efficiency. Lastly, CNN-LSTM combines CNNs for feature extraction and LSTM for sequence processing. It passes the data through a series of 1D convolutional layers followed by a sequence of LSTM layers and an FC layer.

The hyper-parameters of all models were optimized to provide a minimal loss solution over the test set. Specifically for our Transformer-based model, it is trained with a learning rate of 0.001, a weight decay of 5×10^{-5} and batch size of 32. Furthermore, the embedding of the transformer maps into $d_{model} = 32$ dimension space following two layers, each with eight attention heads and a feed-forward network of $d_{ff} = 128$ hidden layers. Finally, the Transformer's output

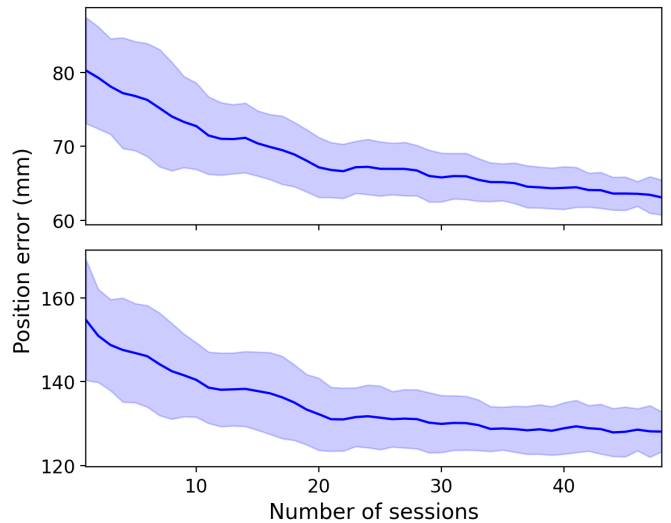


Fig. 5. Position errors of the (top) elbow and (bottom) wrist, with regard to the number of recorded sessions used for training the Transformer-based model. The results show mean and standard deviation values for 15 training attempts while sampling different sessions in each.

is fed into three fully connected networks, each with two hidden layers of size [32, 10] and a dropout rate of 0.2.

Table I summarizes the comparative analysis between the models. The results show the Root Mean Square Error (RMSE) for the elbow and wrist positions over the test data and the mean inference time for a single prediction. For both elbow and wrist, the Transformer provides predictions with the lowest error. Predicting wrist position generally poses more challenges than elbow position due to the greater complexity of wrist movements. This is reflected in the slightly larger error values observed for wrist position estimation. While the Transformer architecture offers better performance compared to other models, it generally requires slightly longer inference times due to its increased complex-

ity. However, the inference time remains sufficiently low and enables real-time applications. Figure 4 shows an example of the predicted elbow and wrist positions along some arm trajectory, based on FMG measurements. The mean position errors for the elbow and wrist along the example path are 65.4 mm and 116.6 mm, respectively.

To assess data requirements and robustness, we conducted an analysis of model performance across varying numbers of recorded sessions. Each session consists of 20,000 FMG samples, and the FMG device was repositioned between sessions to ensure data diversity. To evaluate the impact of dataset size, the Transformer-based model was trained 15 times for each $K \in \{1, \dots, 48\}$ value, using randomly sampled sessions from the dataset. The resulting position errors are presented in Figure 5. The error is reduced with the increase of session data. Notably, elbow and wrist estimation errors approach their final levels with approximately half the total sessions, indicating rapid convergence. Furthermore, the standard deviation across 15 trials decreases with more sessions, suggesting improved model robustness. The observed performance improvements underscore the significance of data variability introduced by repeated device placements, demonstrating the model’s enhanced robustness to variations in positioning and tightening forces.

C. Feature Importance

To assess the relative importance of each FSR sensor, we employed permutation feature importance [39], a common technique for evaluating feature contributions in learned models. By randomly shuffling the values of individual sensor readings and measuring the resulting increase in prediction error, we can quantify the importance of each sensor in the model’s decision-making process. The score is the error computed according to

$$E_i = \frac{e_i - e}{e} \times 100\%, \quad (3)$$

where e is the mean error of the non-permuted model and e_i is the mean error when feature i is permuted. Table II presents the feature importance scores for each FSR sensor on the user’s arm, averaged across wrist and elbow position errors. Sensor placements and importance score heatmap are illustrated in Figure 6. Out of the 32 sensors, 11 were found to be particularly influential, with importance scores exceeding 3%. This suggests that entire rows of FSR sensors can be removed and a more compact FMG device, utilizing a reduced number of sensors, could be designed without significant compromises in accuracy.

D. Model Transfer

To evaluate the model’s generalization capabilities, we tested it on two new participants with different Chest Circumferences (CC), Shoulder Widths (SW) and Upper-Arm Circumferences (UAC), who were not included in the original training dataset. Data was collected from these participants following the same procedure outlined in Section II-C, each having 10,000 labeled samples yielding 4,850 temporal sequences. Table III summarizes the results along

TABLE II
FEATURE IMPORTANCE SCORES OF THE FSR SENSORS ON THE FMG DEVICE.

Sensor Index	Score (%)	Sensor Index	Score (%)	Sensor Index	Score (%)	Sensor Index	Score (%)
1	1.39	9	9.52	17	0.99	25	0.62
2	4.93	10	4.94	18	2.36	26	1.18
3	12.82	11	0.89	19	1.63	27	1.07
4	0.99	12	1.25	20	6.49	28	1.16
5	3.37	13	0.07	21	8.23	29	1.11
6	7.88	14	0.01	22	1.07	30	0.91
7	0.5	15	0.66	23	0.94	31	0.49
8	5.88	16	1.58	24	4.65	32	13.35

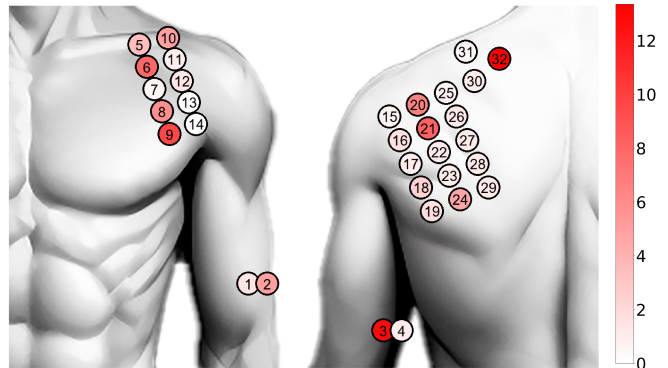


Fig. 6. Sensor locations and heatmap of feature importance scores for the FSR sensors on the FMG device.

with anthropometric measures of all participants including the one used for training. While the model’s accuracy decreased slightly when tested on new participants with different anthropometric measurements, the results demonstrate its ability to generalize and perform effectively. To improve transferability, one can collect data from various users or fine-tune the above model with limited data from the new user.

E. Real-time HRI Demonstration

We have conducted an HRI demonstration in a shared workspace scenario. The Franka collaborative robotic arm was positioned 0.72 meters from a user on a workstation table as seen in Figure 1. The robot was programmed to move in a pre-defined pick-and-place path across the workstation. No cameras were used to estimate the pose of the user. The nominal position of the human torso is assumed to be known. By observing the state of the human arm solely based on FMG measurements, the robot can instantly halt its motion to avoid interfering with the user’s arm path. If a potential

TABLE III
ACCURACY OF MODEL TRANSFER TO NEW USERS

User	CC (mm)	SW (mm)	UAC (mm)	Position error (mm)	
				Elbow	Wrist
Train	98	44	28	61	122
1	99	46	30.5	100	190
2	92	44	25.5	95	186

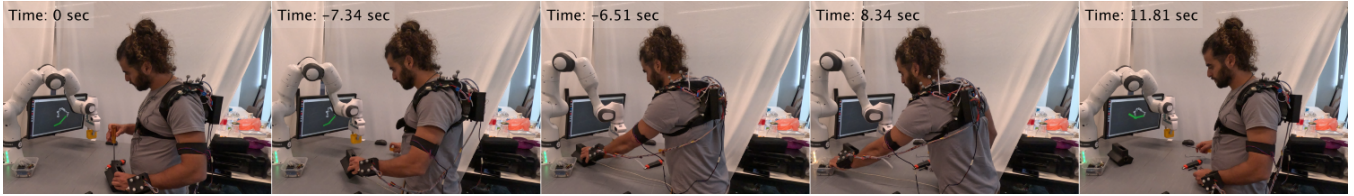


Fig. 7. A user wearing an FMG device interrupts the robot’s motion. The robot pauses its motion based on FMG-based state estimation and resumes only when the user’s arm is no longer in the robot’s path.

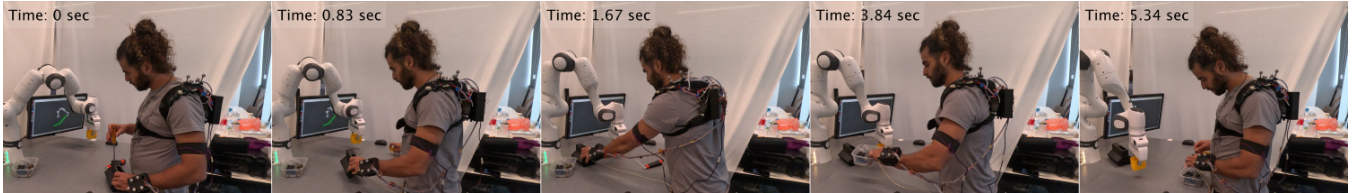


Fig. 8. A user wearing an FMG device puts down an object and picks up a new one in a shared workspace, while crossing the path of the robot. The robot pauses its motion based on FMG-based state estimation and resumes only when the user’s arm is no longer in the robot’s path.

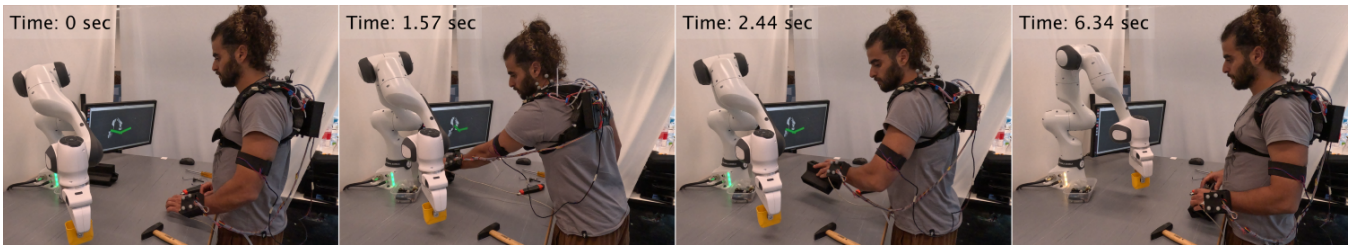


Fig. 9. A user wearing an FMG device picks up an object in a shared workspace, while crossing the path of the robot. The robot pauses its motion based on FMG-based state estimation and resumes only when the user’s arm is no longer in the robot’s path.

TABLE IV
HRI DEMONSTRATION SUCCESS RATES

	Session	
	1	2
Success rate	84%	90%
False positive	5%	10%
False negative	11%	0%

collision with the user arm is detected, the robot will stop its motion until its path is clear. Minimal collision clearance was defined to be 150 mm based on the accuracy of the model.

Two experimental sessions were conducted. In the first session, the user deliberately interfered the motion of the robot by blocking its path. An example of such trial is demonstrated in Figure 7. In the second session, the user naturally performed various tasks, such as picking up and placing tools and other objects scattered on the table (Figures 8-9), while blocking the path of the robot. Each of the sessions consisted of 60 trials. Table IV presents the success rate for the two sessions, including metrics for false positive with failure to stop and false negatives with unnecessary stops. For the latter, a momentary large error made the robot estimate a potential collision leading to a stop. Nevertheless, the majority of trials resulted in true positives, demonstrating the potential of this approach for natural HRI, without visual

perception.

IV. CONCLUSIONS

We investigated the use of a low-cost wearable FMG device for human arm pose estimation in Human-Robot Interaction (HRI) scenarios. This device, worn on the user’s shoulder, incorporates 32 FSR sensors. Using a Transformer-based model, FMG measurements are mapped to the positions of the elbow and wrist, with respect to the shoulder. Our approach exhibited the ability to provide robust and fairly accurate arm pose estimations. Unlike common IMU solutions for arm pose estimation, the FMG device can provide drift-free and absolute estimations without the need for frequent calibrations. The trained model was also shown to be transferable to new users with slight decline in accuracy. Furthermore, a set of HRI experiments has demonstrated the robot’s ability to avoid collisions using the estimated arm poses in a shared workspace. Generally, the FMG device has the potential to enhance various HRI applications, including medical procedures, factory work and assistive technologies.

While the estimation model was shown to be able to fairly generalize to new users, future work should consider making the model more robust to new users. One approach to enhance the model’s generalization capabilities is to train it on a diverse dataset encompassing data from multiple users, as demonstrated in [31]. Alternatively, future work

could involve customizing both the FMG device and the model to individual users. This could include 3D scanning a user's body to create a custom-fitted device, ensuring optimal sensor placement and data quality. Then, the model can be customized for the user through fine-tuning with a limited amount of additional data, as in [26]. In further work, the integration of FSR sensors into wearable textiles could open up new possibilities for advanced and more spontaneous HRI. Future work could also explore the integration of FMG with visual perception to create a robust hybrid system capable of handling diverse environmental conditions.

REFERENCES

- [1] R. Schiavi, A. Bicchi, and F. Flacco, "Integration of active and passive compliance control for safe human-robot coexistence," in *IEEE Inter. Conf. on Robotics and Automation*, 2009, pp. 259–264.
- [2] A. De Luca and F. Flacco, "Integrated control for pHRI: Collision avoidance, detection, reaction and collaboration," in *IEEE RAS EMBS Int. Conf. on Biomedical Robotics and Biomech.*, 2012, pp. 288–295.
- [3] A. M. Okamura, M. J. Matarić, and H. I. Christensen, "Medical and health-care robotics," *IEEE Robotics & Automation Magazine*, vol. 17, no. 3, pp. 26–37, 2010.
- [4] A. Mohebbi, "Human-robot interaction in rehabilitation and assistance: a review," *Current Robotics Reports*, vol. 1, pp. 1–14, 09 2020.
- [5] E. Matheson, R. Minto, E. G. G. Zampieri, M. Faccio, and G. Rosati, "Human–robot collaboration in manufacturing applications: A review," *Robotics*, vol. 8, no. 4, 2019. [Online]. Available: <https://www.mdpi.com/2218-6581/8/4/100>
- [6] C. Qin, A. Song, L. Wei, and Y. Zhao, "A multimodal domestic service robot interaction system for people with declined abilities to express themselves," *Intelligent Service Robotics*, vol. 16, pp. 1–20, 06 2023.
- [7] D. Osokin, "Real-time 2d multi-person pose estimation on cpu: Lightweight openpose," 2018. [Online]. Available: <https://arxiv.org/abs/1811.12004>
- [8] C. Lugaresi, J. Tang, H. Nash, C. McClanahan, E. Uboweja, M. Hays, F. Zhang, C.-L. Chang, M. Yong, J. Lee, W.-T. Chang, W. Hua, M. Georg, and M. Grundmann, "Mediapipe: A framework for perceiving and processing reality," in *Workshop on Computer Vision for AR/VR at IEEE Computer Vision and Pattern Recognition*, 2019.
- [9] B. Schmidt and L. Wang, "Depth camera based collision avoidance via active robot control," *Journal of manufacturing systems*, vol. 33, no. 4, pp. 711–718, 2014.
- [10] A. Toshev and C. Szegedy, "DeepPose: Human pose estimation via deep neural networks," *IEEE Conference on Computer Vision and Pattern Recognition*, 2014.
- [11] Z.-Y. Wang, Z.-R. Xiang, J.-Y. Zhi, T.-C. Ding, R. Zou, and Y.-X. Lan, "Model for predicting the angles of upper limb joints in combination with semg and posture capture," *Measurement Science and Technology*, vol. 35, no. 2, 2024.
- [12] X. Niu, K. Zou, D. Shen, S. Drew, S. Wu, G. Guo, and R. Chen, "Ultramotion: High-precision ultrasonic arm tracking for real-world exercises," *IEEE Transactions on Mobile Computing*, vol. 23, no. 2, pp. 1846–1862, 2024.
- [13] I. Prayudi and D. Kim, "Design and implementation of imu-based human arm motion capture system," in *IEEE International Conference on Mechatronics and Automation*, 2012, pp. 670–675.
- [14] X. Yun and E. R. Bachmann, "Design, implementation, and experimental results of a quaternion-based kalman filter for human body motion tracking," *IEEE Transactions on Robotics*, vol. 22, no. 6, pp. 1216–1227, 2006.
- [15] A. Atrsaei, H. Salarieh, A. Alasty, and M. Abediny, "Human arm motion tracking by inertial/magnetic sensors using unscented kalman filter and relative motion constraint," *Journal of Intelligent & Robotic Systems*, vol. 90, 05 2018.
- [16] S. García-de Villa, D. Casillas-Pérez, A. Jiménez-Martín, and J. J. García-Domínguez, "Inertial sensors for human motion analysis: A comprehensive review," *IEEE Transactions on Instrumentation and Measurement*, vol. 72, pp. 1–39, 2023.
- [17] M. Dumpis, D. Gedminas, and A. Serackis, "Inertial sensor based system for upper limb motion quantification," in *IEEE Open Conference of Electrical, Electronic and Information Sciences*, 2022, pp. 1–6.
- [18] N. DeVrio, V. Mollyn, and C. Harrison, "Smartposer: Arm pose estimation with a smartphone and smartwatch using uwb and imu data," in *ACM Symposium on User Interface Software and Technology*. Association for Computing Machinery, 2023.
- [19] J.-W. Cui, Z.-G. Li, H. Du, B.-Y. Yan, and P.-D. Lu, "Recognition of upper limb action intention based on imu," *Sensors*, vol. 22, 03 2022.
- [20] N. D. Kahanowich and A. Sintov, "Learning human-arm reaching motion using a wearable device in human–robot collaboration," *IEEE Access*, vol. 12, pp. 24 855–24 865, 2024.
- [21] O. Amft, H. Junker, P. Lukowicz, G. Troster, and C. Schuster, "Sensing muscle activities with body-worn sensors," in *Int. Workshop on Wearable and Implantable Body Sensor Networks*, 2006, pp. 4–pp.
- [22] X. Jiang, L.-K. Merhi, Z. G. Xiao, and C. Menon, "Exploration of force myography and surface electromyography in hand gesture classification," *Med. Engineering & Physics*, vol. 41, pp. 63–73, 2017.
- [23] A. Belyea, K. Englehart, and E. Scheme, "FMG versus EMG: A comparison of usability for real-time pattern recognition based control," *IEEE Trans. on Biomed. Eng.*, vol. 66, no. 11, pp. 3098–3104, 2019.
- [24] Z. Zheng, Z. Wu, R. Zhao, Y. Ni, X. Jing, and S. Gao, "A review of EMG-, FMG-, and EIT-based biosensors and relevant human–machine interactivities and biomedical applications," *Biosensors*, vol. 12, no. 7, 2022.
- [25] H. K. Yap, A. Mao, J. C. H. Goh, and C. Yeow, "Design of a wearable FMG sensing system for user intent detection during hand rehabilitation with a soft robotic glove," in *IEEE Int. Conf. on Biomedical Rob. and Biomech.*, 2016, pp. 781–786.
- [26] A. Mizrahi and A. Sintov, "TeleFMG: A wearable force-myography device for natural teleoperation of multi-finger robotic hands," *IEEE Robotics and Automation Letters*, vol. 9, no. 3, pp. 2933–2940, 2024.
- [27] A. Radmand, E. Scheme, and K. Englehart, "High-density force myography: A possible alternative for upper-limb prosthetic control," *J. of Rehabilitation Res. and Dev.*, vol. 53, no. 4, pp. 443–456, 2016.
- [28] E. Cho, R. Chen, L.-K. Merhi, Z. Xiao, B. Pousett, and C. Menon, "Force myography to control robotic upper extremity prostheses: a feasibility study," *Frontiers in bioengineering and biotechnology*, vol. 4, p. 18, 2016.
- [29] J. Gantenbein, C. Ahmadzadeh, O. Heeb, O. Lambercy, and C. Menon, "Feasibility of force myography for the direct control of an assistive robotic hand orthosis in non-impaired individuals," *J NeuroEngineering and Rehabilitation*, vol. 20, no. 101, 2023.
- [30] N. D. Kahanowich and A. Sintov, "Robust classification of grasped objects in intuitive human-robot collaboration using a wearable force-myography device," *IEEE Robotics and Automation Letters*, vol. 6, no. 2, pp. 1192–1199, 2021.
- [31] E. Bamani, N. D. Kahanowich, I. Ben-David, and A. Sintov, "Robust multi-user in-hand object recognition in human-robot collaboration using a wearable force-myography device," *IEEE Robotics and Automation Letters*, vol. 7, no. 1, pp. 104–111, 2022.
- [32] G. Zerveas, S. Jayaraman, D. Patel, A. Bhamidipaty, and C. Eickhoff, "A transformer-based framework for multivariate time series representation learning," in *ACM SIGKDD Conference on Knowledge Discovery & Data Mining*, 2021, p. 2114–2124.
- [33] T. GC and C. TM, "Functional anatomy of the shoulder," *J Athl Train*, vol. 35, no. 3, pp. 248–55, 2000.
- [34] M. Anvaripour, M. Khoshnam, C. Menon, and M. Saif, "Fmg- and rnn-based estimation of motor intention of upper-limb motion in human-robot collaboration," *Frontiers in Robotics and AI*, vol. 7, 2020.
- [35] R. Liaw, E. Liang, R. Nishihara, P. Moritz, J. E. Gonzalez, and I. Stoica, "Tune: A research platform for distributed model selection and training," *arXiv preprint arXiv:1807.05118*, 2018.
- [36] S. Kiranyaz, O. Avci, O. Abdeljaber, T. Ince, M. Gabbouj, and D. J. Inman, "1d convolutional neural networks and applications: A survey," *Mechanical Systems and Signal Processing*, vol. 151, p. 107398, 2021.
- [37] A. Zeng, M. Chen, L. Zhang, and Q. Xu, "Are transformers effective for time series forecasting?" in *AAAI Conf. on Artificial Intel.*, 2023.
- [38] T. N. Sainath, O. Vinyals, A. Senior, and H. Sak, "Convolutional, long short-term memory, fully connected deep neural networks," in *IEEE International Conference on Acoustics, Speech and Signal Processing (ICASSP)*, 2015, pp. 4580–4584.
- [39] J. Yang, K.-Q. Shen, C. Ong, and X.-P. Li, "Feature selection for mlp neural network: The use of random permutation of probabilistic outputs," *IEEE Trans. on Neural Net.*, vol. 20, pp. 1911 – 1922, 2010.